Influence of the Meniscus Force for Contact Recording Head Dynamics Over a Randomly Undulating Disk Surface

Hiroshige Matsuoka, Shigehisa Fukui, and Takahisa Kato

***Abstract*—Dynamic characteristics of a tripad contact recording head over a random undulation disk surface are analyzed considering the surface energy of a thin liquid film lubricant. The head-suspension assembly is described in terms of a three-degrees-of-freedom (3-DOF) model. The configuration of the contact pad, the lubricant, and the disk surface is classified into four regimes, and the equations of motion for each regime considering the meniscus force and the contact force are solved. It is clarified from the simulation and multiple regression results that the surface energy has significant effects on the dynamics of the contact slider.**

***Index Terms*—Contact slider, three-degrees-of-freedom (3-DOF) model, meniscus force, surface energy.**

I. Introduction

RECORDING density of hard disk drives (HDDs) becomes larger to meet the demand of larger capacity. In the near future, the recording density will run up to 100 Gbit/in^2 [1], [2] though that of current HDD is about several tens of Gbit/in^2. There are several points to be improved for the large recording density, and the reduction of the spacing between a head and a disk surface is considered the most important. The flying height of a magnetic head over a disk surface has approached 12–14 nm which would be the smallest limit realized for the reduction of the spacing in the flying head system. Then, a contact head slider/disk interface (HDI) system is proposed as a substitute for the flying head system [3], [4].

Two kinds of sliders in the contact HDI system are introduced so far, namely, a near-contact slider (i.e., intermittent or partial contact slider) and in-contact slider. In the years ahead, it is considered that the flying HDI system will shift to the near-contact system, then to the in-contact system.

The design method of the in-contact HDI system is quite different from that of the flying or the near-contact HDI systems : while the flying or the near-contact HDI systems are designed by using the gas-flow equation because the slider is kept flying by the gas flow between the slider and the disk [5], [6], on the other hand, the contact effects of the solid disk surface or the liquid lubricant upon the disk is important in the in-contact HDI system. In the past, several studies on the in-contact HDI system were carried out [7]–[10]. These past studies, however, scarcely took into account the lubricant on the disk surface. It was reported in experimental studies that the lubricant played a very important role to the dynamic characteristics of a head slider in the in-contact HDI system. In particular, they pointed out that even a thin lubricant diminishes the bouncing motion of a head slider [11]. The authors reported the basic characteristics of dynamics of a contact slider over a sinusoidal undulation [12].

Manuscript received June 20, 2002. This work was supported in part by a grant from Storage Research Consortium (SRC).

H. Matsuoka and S. Fukui are with Department of Applied Mathematics and Physics, Faculty of Engineering, Tottori University, Tottori 680-8552, Japan (e-mail: hiro@damp.tottori-u.ac.jp; fukui@damp.tottori-u.ac.jp).

T. Kato is with the Institute of Mechanical Systems Engineering, AIST, Ibaraki 305-8564, Japan (e-mail: kato.t@aist.go.jp).

Digital Object Identifier 10.1109/TMAG.2003.808942

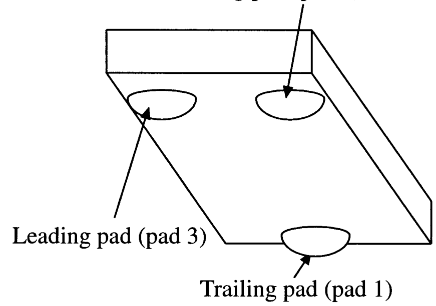

Fig. 1. Tripad slider with spherical pads.

In this study, calculation results of behavior of a contact recording head over a random undulation disk surface are described using a computer simulation program for the slider motion where a three-degrees-of-freedom (3-DOF) model of head-suspension assembly is introduced and the effects of meniscus force due to the meniscus bridge between the slider and the disk are considered [12]–[14]. The influence of the surface energy of the liquid lubricant on dynamics of the head is investigated by the multiple regression method.

II. Equations of Motion

The tripad slider shown schematically in Fig. 1 [15] is modeled three dimensionally as shown in Fig. 2. The tripad slider has two leading pads and one trailing pad, and forces, i.e., meniscus force, contact force from disk, friction force, act only on the bottom of these three contacting pads. The authors consider the spherical pads in this study for the sake of simple estimation of the meniscus force. The axes, z, θ, and ϕ, represent bouncing, pitching, and rolling direction, respectively, and the equations of motion are obtained for these three directions. The axes x and y represent sliding and seeking directions of the head slider, respectively. The head slider-suspension assembly has spring and damper structure in each direction, i.e., k_s, c_s, k_θ, c_θ, k_φ, c_φ,

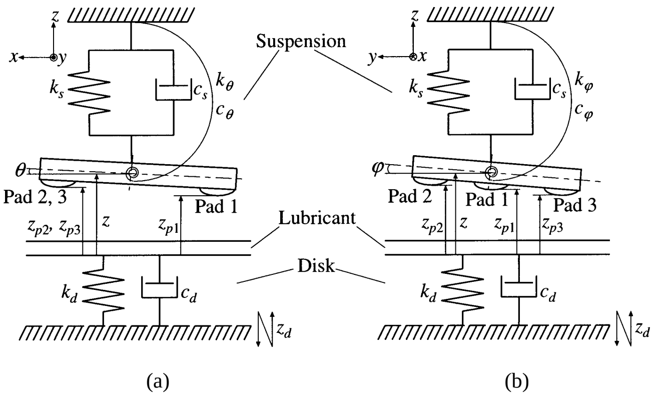

Fig. 2. Three-degrees-of-freedom model of a head-suspension assembly: (a) side view and (b) front view.

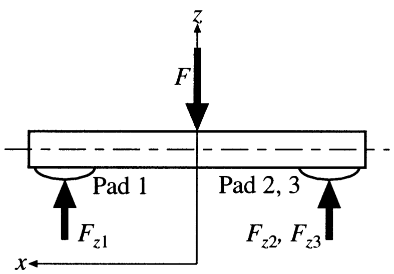

Fig. 3. A model of bouncing (z) direction.

and the disk is assumed to be a flexible body characterized with linear spring k_d and damper c_d.

In deriving equations of motion, we take F_{xi}, F_{yi}, and F_{zi} for force elements acting on ith pad $(i = 1, 2, 3)$ and the forces are described in Section III.

As the equations of motion are described in detail [12]–[14], final expressions are written here.

A. Bouncing (z) Direction

$$m\ddot{z} + c_s\dot{z} + k_s z = -F + F_{z1} + F_{z2} + F_{z3} \tag{1}$$

where m is mass of slider and F is load on the slider (see Fig. 3).

B. Pitching (θ) Direction

$$\begin{aligned} I_\theta\ddot{\theta} + c_\theta\dot{\theta} + k_\theta\theta = &- l_{p1}\cos\Psi_{p1}F_{z1} \\ &+ l_{p1}\sin\Psi_{p1}F_{x1} \\ &+ l_{p2}\cos\Psi_{p2}F_{z2} \\ &- l_{p2}\sin\Psi_{p2}F_{x2} \\ &+ l_{p3}\cos\Psi_{p3}F_{z3} \\ &- l_{p3}\sin\Psi_{p3}F_{x3} \end{aligned} \tag{2}$$

where $l_{pi} (i = 1, 2, 3)$ denotes length of a line perpendicular to the y axis drawn from the bottom of the ith pad, Ψ_{pi} denotes the angle between the xy plane and a line perpendicular to the y axis drawn from the bottom of the ith pad, moment of inertia is $I_\theta = ma^3/3$ (see Fig. 4), and a is the slider length.

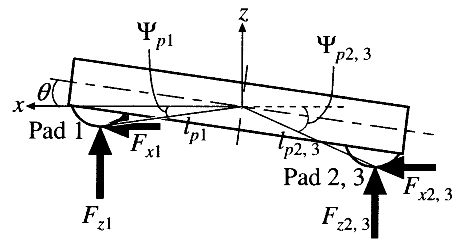

Fig. 4. A model of pitching (θ) direction.

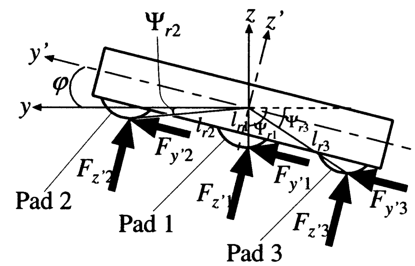

Fig. 5. A model of rolling (φ) direction.

C. Rolling (φ) Direction

$$\begin{aligned} I_\varphi\ddot{\varphi} + c_\varphi\dot{\varphi} + k_\varphi\varphi = &- l_{r1}\cos(\varphi - \Psi_{r1})F_{z'1} \\ &- l_{r1}\sin(\varphi - \Psi_{r1})F_{y'1} \\ &+ l_{r2}\cos(\varphi - \Psi_{r2})F_{z'2} \\ &+ l_{r2}\sin(\varphi - \Psi_{r2})F_{y'2} \\ &- l_{r3}\cos(\varphi - \Psi_{r3})F_{z'3} \\ &- l_{r3}\sin(\varphi - \Psi_{r3})F_{y'3} \end{aligned} \tag{3}$$

where l_{ri} denotes length of a line perpendicular to the x' axis drawn from the bottom of the ith pad, Ψ_{ri} denotes the angle between xy plane and a line perpendicular to the x axis drawn from the bottom of the ith pad, moment of inertia is $I_\Psi = mc^3/3$ (see Fig. 5), c is slider width, and

$$\begin{pmatrix} F_{x'i} \\ F_{y'i} \\ F_{z'i} \end{pmatrix} = \begin{pmatrix} \cos\theta & 0 & \sin\theta \\ -\sin\theta & \sin\varphi\cos\varphi & \cos\theta\sin\varphi \\ -\sin\theta\cos\varphi & -\sin\varphi\cos\varphi & \cos\varphi \end{pmatrix} \times \begin{pmatrix} F_{xi} \\ F_{yi} \\ F_{zi} \end{pmatrix}. \tag{4}$$

In this manner, we get equations of motion for three-dimensional in-contact HDI system.

III. Forces Acting on the Pad

The authors consider four regimes with respect to configuration of a pad, lubricant, and disk surface as shown in Fig. 6. Note that the meniscus bridge is formed and the meniscus force acts on the pad in case of diving, contacting, and jumping regimes. In past studies on the meniscus force in the field of HDI, the stiction of a head slider in contact start/stop (CSS) is mainly discussed [16], [17]. These past studies, however, take the static meniscus force at the CSS into account, and there are scarcely

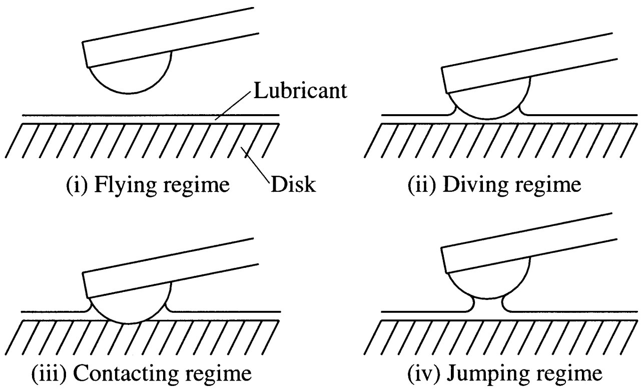

Fig. 6. Four regimes of head-lubricant-disk interface.

studies on the effects of meniscus force of the lubricant on dynamic characteristics of an in-contact head slider. Final expressions are written here since forces acting on the pads at the each regime are described in detail in [12]–[14]

A. Flying Regime

$$F_x^f = F_y^f = F_z^f = 0 \tag{5}$$

where superfix f denotes flying regime.

B. Diving Regime

$$\begin{cases} F_x^d = F_y^d = 0 \\ F_z^d = -2\pi R\gamma(1+\cos\theta_c) \end{cases} \tag{6}$$

where superfix d denotes diving regime, R is the radius of curvature of the spherical pad, γ is the surface energy of the liquid lubricant, and θ_c is the contact angle.

C. Contacting Regime

The pad comes into contact with both lubricant and disk. Contact force F_c with the disk is

$$F_c = c_d(\dot{z}_d - \dot{z}_p) + k_d(z_d - z_p) \tag{7}$$

where z_p is the coordinate of the bottom of the pad in the z axis, and z_d is the displacement of the disk by the undulation. Then, forces in this regime are given by

$$\begin{cases} F_x^c = -\mu\left\{c_d(\dot{z}_d - \dot{z}_p) + k_d(z_d - z_p)\right\}\cos\kappa \\ F_y^c = -\mu\left\{c_d(\dot{z}_d - \dot{z}_p) + k_d(z_d - z_p)\right\}\sin\kappa \\ F_z^c = c_d(\dot{z}_d - \dot{z}_p) + k_d(z_d - z_p) - 2\pi R\gamma(1+\cos\theta_c) \end{cases} \tag{8}$$

where superfix c denotes the contacting regime, $\kappa = \tan^{-1}(U/V)$, U is the seek speed, and V is the disk velocity.

D. Jumping Regime

$$\begin{cases} F_x^j = -2\pi R\gamma(1+\cos\theta_c)\left(1 - \frac{2d}{\sqrt{4d^2+R^2\phi_0^4}}\right)\sin\xi\cos\kappa \\ F_y^j = -2\pi R\gamma(1+\cos\theta_c)\left(1 - \frac{2d}{\sqrt{4d^2+R^2\phi_0^4}}\right)\sin\xi\sin\kappa \\ F_z^j = -2\pi R\gamma(1+\cos\theta_c)\left(1 - \frac{2d}{\sqrt{4d^2+R^2\phi_0^4}}\right)\cos\kappa \end{cases} \tag{9}$$

where ξ is incline angle of the meniscus bridge, superfix j denotes jumping regime, d is the distance between the lubricant's surface and pad, and ϕ_0 is a filling angle of the meniscus bridge at $d = 0$ (details are written [12]).

Concerning the formation of the meniscus bridge, the authors assumed that the meniscus bridge forms instantaneously when the bottom of a pad touches the lubricant on the surface and breaks when the diameter of minimum horizontal sectional circle of the bridge diminishes due to the elongation.

IV. Contact Stiffness and Contact Pressure

Assuming that the contact between the spherical pad and the disk is Hertzian, the contact stiffness k_d is given by [18]

$$k_d = \frac{W}{\delta} \tag{10}$$

where W is the sum of the load F and the meniscus force F_m, δ is the center indentation depth and equals $a_H^2/2R$, a_H is the radius of the Hertzian contact circle and equals $(3WR/4E)^{1/3}/2^{1/6})$, and E is the equivalent Young's modulus defined as

$$\frac{2}{E} = \frac{1-\nu_s^2}{E_s} + \frac{1-\nu_d^2}{E_d} \tag{11}$$

where E_s and E_d are Young's modulus of the slider and the disk, respectively, ν_s and ν_d are Poisson's ratio of the slider and the disk, respectively. The authors adopted the value of these material constants as the following: $E_s = 385$ GPa, $E_d = 70.4$ GPa, $\nu_s = \nu_d = 0.3$, assuming that the head slider and the disk are made of AlTiC and glass [8]. For example, $k_d = 4.17 \times 10^5$ N/m when the load is 1 mN and the surface energy of lubricant is 25 mJ/m^2. In this study, the value of the contact stiffness at the static contact force is used in the whole calculation, though the contact stiffness between the spherical pad and the plane disk changes nonlinearly by the indentation depth, i.e., the contact force [19].

The contact force F_c at the contacting regime is given by (7) and the contact pressure p_c is

$$p_c = \frac{F_c}{\pi a_H^2} \tag{12}$$

which means average pressure in the Hertzian contact.

V. Calculation Method and Conditions

The equations of motion are computed by means of the Runge–Kutta–Gill (RKG) method. The time step dt in the RKG method is varied such that $dt = 10^{-9}$ s for the flying and the diving regime, 10^{-10} s for the contacting regime, and 2×10^{-12} s for the jumping regime. The simulator makes the time step smaller and recalculates the position of the pads automatically in order to calculate accurately when the regime at some pads changed. The initial conditions at $t = 0$ are given as $\dot{z} = \theta = \dot{\theta} = \varphi = \dot{\varphi} = 0$ and $z(t = 0)$ is determined so that one pad which is on the highest disk surface comes into contact with the disk surface.

Note that the behavior of the trailing pad (pad 1 as shown in Figs. 1 and 2) where the magnetic head is attached is investigated in this study. In the following calculation results, values of parameters are shown in [12]–[14].

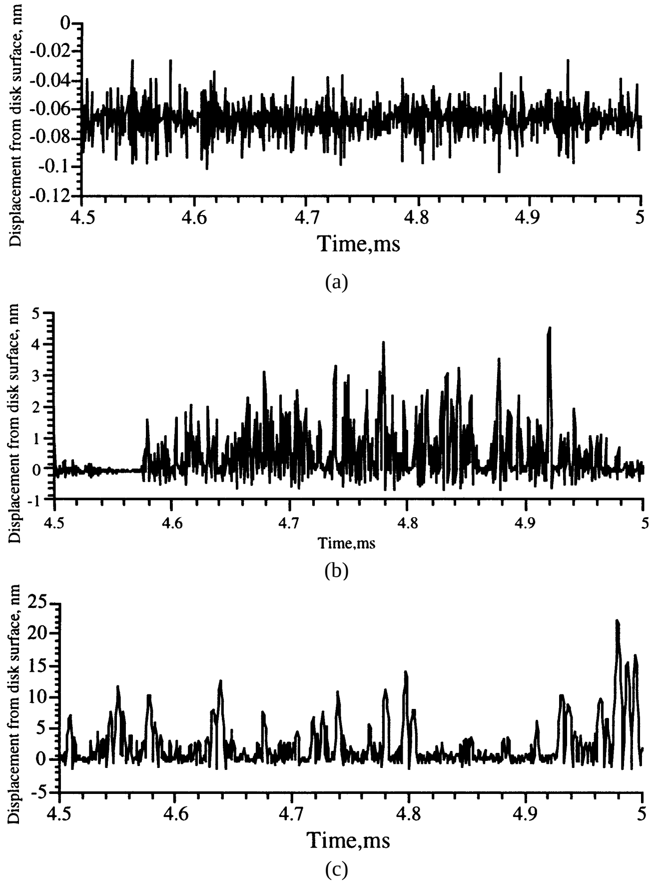

Fig. 7. Bouncing height of pad 1 in time domain: (a) $\lambda^* = 80$; (b) $\lambda^* = 10$; and (c) $\lambda^* = 4$.

VI. Results for Random Undulation

The moving average method [20] is used in order to generate random undulation of the disk. The random rough surface is obtained by two parameters, i.e., rms value of the undulation amplitude and the nondimensional correlation length λ^*, where $\lambda^* = \lambda/\Delta x = \lambda/\Delta y$, λ is correlation length, Δx and Δy are distance between grid points, and $\Delta x = \Delta y = 2\ \mu$m. The nondimensional correlation length λ^* corresponds to the inverse of wavy frequency in the case of sinusoidal undulation [12], [13]. The authors assume that the distribution of the surface height is Gaussian and the undulation is homogeneous. The examples of a disk surface with random undulation obtained by this method are shown in [13].

In this section, some examples of the simulation results are shown and the details are written [13].

A. Bouncing Height in Time Domain

Fig. 7(a)–(c) shows examples of the calculation results of bouncing height of pad $1(z_1)$ in time domain. It is found that pad 1 comes into complete contact with the surface of the correlation length in the case of $\lambda^* = 80$ [Fig. 9(a)] but bounce appears in the case of $\lambda^* = 10$ and 4 [Fig. 9(b) and (c)]. Maximum bouncing heights in each condition are -0.0135 nm for $\lambda^* = 80$, 4.60 nm for $\lambda^* = 10$, and 22.7 nm for $\lambda^* = 4$. Note that the correlation length, λ^*, corresponds to the inverse of the wavy frequency in the case of the sinusoidal undulation, i.e., the smaller value of λ^* means the larger value of the wavy

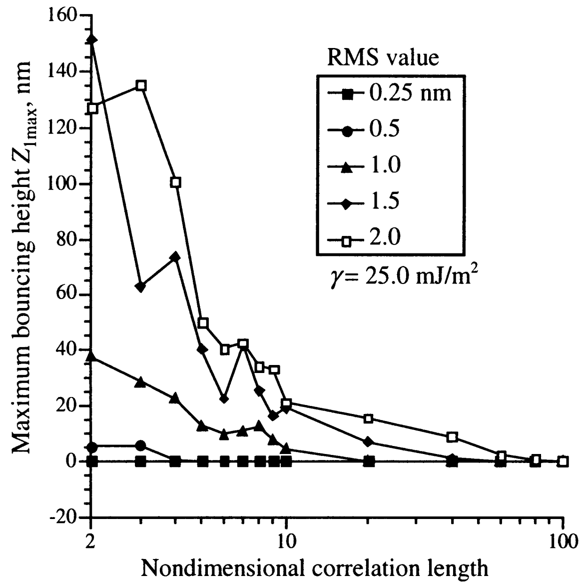

Fig. 8. Nondimensional correlation length and maximum bouncing height varying RMS value.

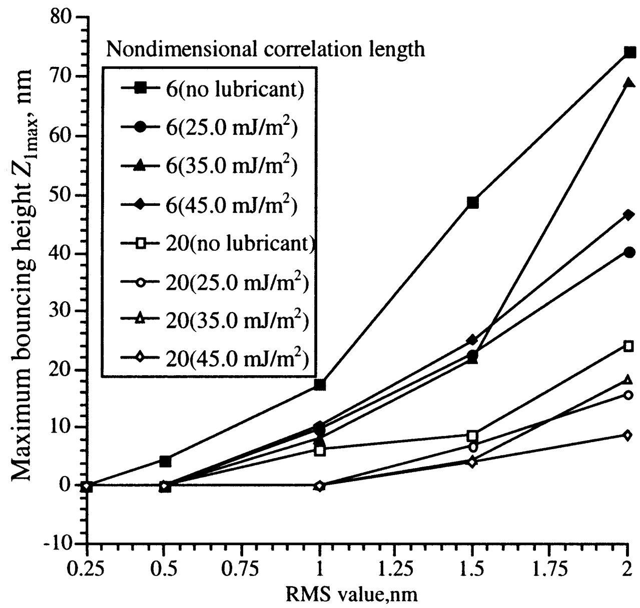

Fig. 9. Effect of RMS value varying nondimensional correlation length and surface energy.

frequency and, therefore, these results are reasonable. A similar tendency was shown also in the case of sinusoidal undulation [12]. The negative value of the displacement from the disk surface means the pad is perfectly contacting with the disk surface and the Herzian contact is occurred.

B. Effect of RMS Value of Disk Undulation

Fig. 8 shows an example of the relation between the nondimensional correlation length and the maximum bouncing height $(z_{1\,\max})$ varying the rms value, and Fig. 9 shows the effect of the rms value of disk undulation on the maximum bouncing height varying the nondimensional correlation length and surface energy. It is seen from these figures that complete contact is realized for all nondimensional correlation length when the rms value is 0.25 nm, but the maximum bouncing height becomes

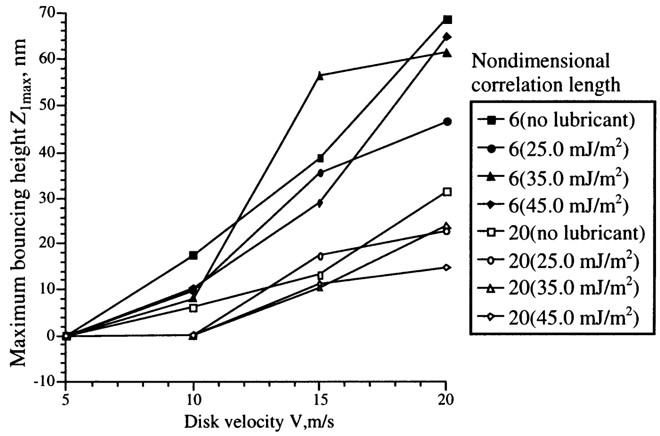

Fig. 10. Effect of disk velocity varying nondimensional correlation length and surface energy.

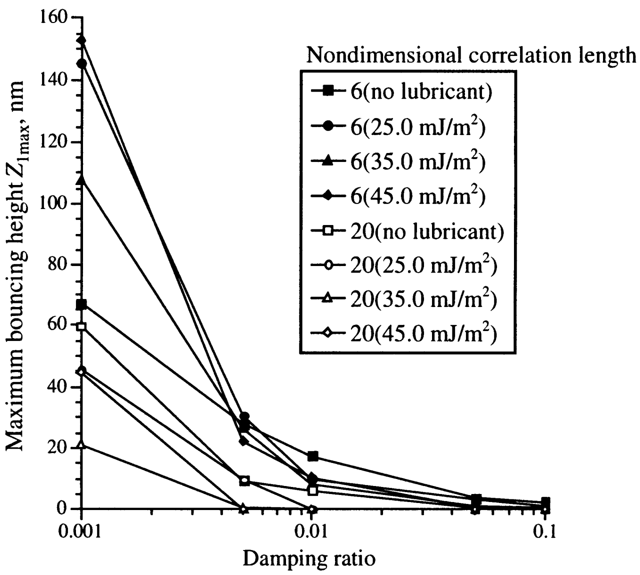

Fig. 11. Effect of contact damping ratio varying nondimensional correlation length and surface energy.

large rapidly when the rms value is 1.5 or 2 nm. The effect of the rms value on the bouncing height is remarkable. Also, it is seen from Fig. 9 that the surface energy, i.e., the meniscus force, can reduce the maximum bouncing height. Note that the line crossing shown in Figs. 8 and 9 is due to the nonlinear characteristics of the governing equations of motion (see Sections II and III), i.e., the head slider shows chaotic behavior when the bouncing occurred.

C. Effect of Disk Velocity

Fig. 10 shows the effect of the disk velocity on the maximum bouncing height varying the nondimensional correlation length and the surface energy. It is found that the maximum bouncing height becomes large when the disk velocity is large. The rotational speed of the HDD has become higher and higher in recent years for high access speed to data and some HDDs have 15 000 rpm (about 31 m/s at a 20-mm disk radius). It is seen from these calculation results that an increase in rotational speed is very disadvantageous for design of in-contact HDI system and it is

TABLE I
MULTIPLE REGRESSION COEFFICIENTS FOR $z_{1\,\max} < 10$ nm

i =	k =	1	2
		Obtained from maximum bouncing height	Obtained from maximum contact pressure
1	RMS value	3.37	0.067
2	Disk velocity	2.41	0.046
3	Nondimensional correlation length	-2.03	-0.049
4	Contact damping ratio	-1.20	-0.031
5	Mass of slider	1.47	0.035
6	Load	-0.21	0.058
7	Surface energy of lubricant	-2.73	0.168
8	Thickness of lubricant	-0.25	0.005

necessary to try to reduce the bouncing height in terms of optimizing other parameters.

D. Effect of Contact Damping Ratio

Fig. 11 shows the effect of the contact damping ratio on the maximum bouncing height varying the nondimensional correlation length and surface energy. The maximum bouncing height is small in case of large damping ratio. Though the contact damping ratio of a real disk is difficult to know, it may be very small considering the disk surface is covered with thin DLC film. Therefore, the device for obtaining large contact damping ratio is necessary, for example, the use of a lubricant with high viscosity is recommended.

Note that the relations between the nondimensional correlation length and the maximum bouncing height show the same tendency as in the case of the rms value, i.e., Fig. 8, when the disk velocity and the damping ratio are varied.

VII. MULTIPLE REGRESSION COEFFICIENTS

The multiple regression was carried out with respect to the bouncing height and the contact pressure in order to investigate the effects of each parameter. We consider the bouncing height and the contact pressure are dependent parameters, y_1, y_2, respectively, and other parameters are independent parameters $x_i (i = 1, 2, \ldots, 8)$, i.e., x_1: rms value, x_2: disk velocity, x_3: nondimensional correlation length, x_4: contact damping ratio, x_5: mass of slider, x_6: load, x_7: surface energy of lubricant, and x_8: thickness of lubricant. In order to minimize the prediction error, we chose the parameters $Y_k = \log y_k (k = 1, 2)$, $X_i = \log x_i (i = 1, 2, \ldots, 8)$. Then, the multiple regression expression is given by

$$Y_k = a_{0k} + \sum_{i=1}^{8} a_{ik} X_i, \quad (k = 1, 2; i = 1, 2, \ldots, 8). \quad (13)$$

The simulation results of the maximum bouncing height $z_{1\,\max} < 10$ nm are used to obtain the multiple regression coefficients a_{ik} because consideration of the large value of $z_{1\,\max}$ is meaningless for the contact recording head. The

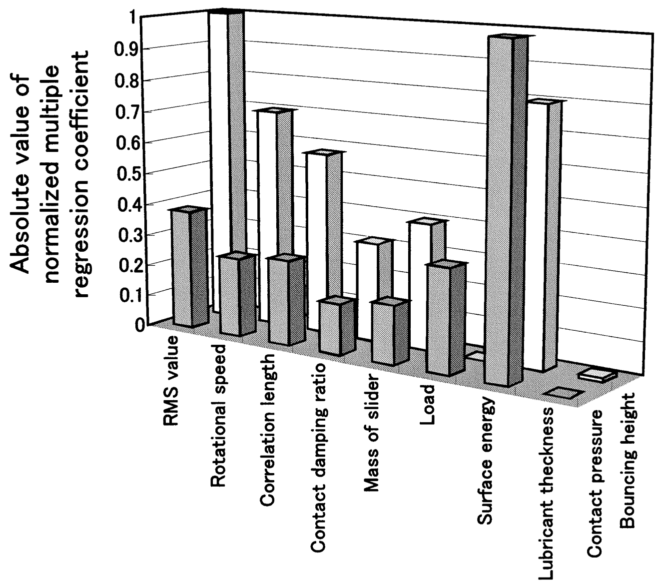

Fig. 12. Absolute values of the multiple regression coefficients which are normalized by the maximum value.

obtained multiple regression coefficients are tabulated in Table I. The multiple correlation coefficient is 0.94 and 0.97 for the maximum bouncing height and the maximum contact pressure, respectively, which means the multiple regression is successful by using (13). The negative value, e.g., -0.21 at the load-maximum bouncing height cell, means that the maximum bouncing height will decrease when the load increases. The design parameters which have different sign coefficients between the maximum bouncing height and the maximum contact pressure, i.e., load, surface energy of lubricant, and thickness of lubricant, are considered to have optimum values as the authors pointed out in the case of a disk surface with sinusoidal undulation [14].

The absolute values of the multiple regression coefficients are shown in Fig. 12, in which the bright bars and the dark bars show the coefficients with respect to the maximum bouncing height and the contact pressure, respectively. Note that the coefficients are normalized by the maximum value. It is found that the RMS value of the undulation amplitude influences the maximum bouncing height most significantly and the next is the surface energy. In the case of the contact pressure, the surface energy has the most significant effect. Therefore, it is very important to take the surface energy of lubricant into account in order to design the contact HDI system. Note that numerical values of these results shown in this paper depend on the mechanical and geometrical model.

VIII. Summary

Dynamic characteristics of a tripad contact recording head over a random undulation disk surface were analyzed considering the surface energy of thin liquid film lubricant. The equations of motion for four regimes considering the meniscus force and the contact force were solved using the RKG method. It was clarified from the simulation results and the multiple regression coefficients that the surface energy has significant effects on the dynamics of the contact head slider.

Acknowledgment

The authors would thank Mr. Masahiro Suwa at Hitachi Systems and Services and Mr. S. Watanabe at Toyo Engineering for programming.

References

[1] *Proc. Symp. Interface Tribology Toward 100 Gbit/in*^{2}, C. S. Bhatia, A. A. Polycarpou, and A. K. Menon, Eds., 1999.
[2] *Proc. Symp. Interface Tribology Toward 100 Gbit/in*^{2} *and Beyond*, C. S. Bhatia, A. A. Polycarpou, and A. K. Menon, Eds., 2000.
[3] H. Hamilton, R. Anderson, and K. Goodson, "Contact perpendicular recording on rigid media," *IEEE Trans. Magn.*, vol. 27, pp. 4921–4926, Sept. 1991.
[4] H. Hamilton, "Perpendicular contact recording on rigid media," *J. Mag. Soc. Japan*, vol. 18, no. S1, pp. 171–178, 1994.
[5] S. Fukui and R. Kaneko, "Analysis of ultrathin gas film lubrication based on linearized boltzmann equation: First report—Derivation of a generalized lubrication equation including thermal creep flow," *ASME J. Trib.*, vol. 110, pp. 253–262, 1988.
[6] D. A. Bailey, "Limits of reynolds equation for negative pressure sliders," *IEEE Trans. Magn.*, vol. 31, pp. 2979–2981, July 1995.
[7] K. Ono, H. Yamaura, and T. Mizokoshi, "Analysis of dynamic contact behavior and tracking characteristics of a single-degree-of-freedom slider model for a contact recording head," *J. JSME C*, vol. 60, pp. 2574–2581, 1994.
[8] K. Ono, K. Takahashi, and K. Iida, "Computer analysis of bouncing vibration and tracking characteristics of a point contact slider model over random disk surfaces," *ASME J. Trib.*, vol. 121, pp. 587–595, 1999.
[9] R. Tsuchiyama, "Simulation of dynamic characteristics of head-disk interface subjected to wavy excitation and collision in contact magnetic recording," *J. JSME C*, vol. 64, pp. 4791–4797, 1998.
[10] K. Iida and K. Ono, "Analysis of bouncing vibrations of a 2-DOF model of tripad contact slider over a random wavy disk surface," *ASME J. Trib.*, vol. 123, pp. 159–167, 2001.
[11] A. Sato, K. Ajiki, M. Yanagisawa, and Y. Tsukamoto, "Head-Disk interface design for in-contact recording using wet systems," *IEEE Trans. Magn.*, vol. 33, pp. 3163–3165, Sept. 1997.
[12] T. Kato, S. Watanabe, and H. Matsuoka, "Dynamic characteristics of an in-contact headslider considering meniscus force: Part 1—Formulation and application to the disk with sinusoidal undulation," *ASME J. Trib.*, vol. 122, pp. 633–638, 2000.
[13] ——, "Dynamic characteristics of an in-contact headslider considering meniscus force: Part 2—Application to the disk with random undulation and design conditions," *ASME J. Trib.*, vol. 123, pp. 168–174, 2001.
[14] H. Matsuoka, S. Fukui, and T. Kato, "Dynamic characteristics of an in-contact head slider considering meniscus force: Part 3—Wear durability and optimization of surface energy of liquid lubricant under perfect contact condition," *ASME J. Trib.*, vol. 124, pp. 801–810, 2002.
[15] M. Yanagisawa, A. Sato, and K. Ajiki, "Bouncing properties for contact sliders," *JSME Proc. IIP '96*, pp. 15–16, 1996.
[16] H. Tian and T. Matsudaira, "The role of relative humidity, surface roughness and liquid build-up on static friction behavior of the head/disk interface," *ASME J. Trib.*, vol. 115, pp. 28–35, 1993.
[17] X. Tian and B. Bhushan, "The micro-meniscus effect of a thin liquid film on the static friction of rough surface contact," *J. Phys. D*, vol. 29, pp. 163–178, 1996.
[18] Y. Yamamoto and M. Kaneta, *Tribology* (in Japanese). Tokyo: Rikogakusya, 1998.
[19] K. Iida and K. Ono, "Effects of slider mass, contact stiffness and contact damping on contact force of a single-DOF contact slider model," *J. JSME C*, vol. 64, pp. 2894–2902, 1998.
[20] J. A. Ogilvy, *Theory of Wave Scattering from Random Rough Surface*. Philadelphia, PA: Institute of Physics, 1991.